JOURNAL OF PROPULSION AND POWER
Vol. 13, No. 2, March–April 1997

Partially Premixed Laminar Gas Flames from Triangular Burners

S. R. Gollahalli* and Samir Subba†
University of Oklahoma, Norman, Oklahoma 73019

An experimental study of the effects of using triangular burner exit ports in place of the standard circular ports in a laminar partially premixed gas burner is presented. A natural gas burner employed in a small residential-scale heating system rated at 5.86 kW was modified. Air entrainment into the nonburning jets, emission indices of nitrogen oxides and carbon monoxide, and inflame temperature and composition profiles were measured. Flowfield in the near-nozzle region was visualized by shadowgraphy. Results show that triangular ports increase air entrainment by 30%, decrease nitrogen oxides emission by less than 15%, and increase carbon monoxide emission by 20%. The effects are explained in terms of the changes in flow structure and instabilities caused by the noncircular geometry and sharp corners of the burner exit port.

Nomenclature

D	=	area equivalent diameter of burner exit port
EI	=	emission index
HHV	=	heating value
M	=	molecular weight
n	=	number of moles
PA	=	primary air
r	=	radial distance from the centroid
SA	=	secondary air
T	=	temperature
Tri	=	triangular port
X	=	mole fraction

Subscripts

a	=	air
f	=	fuel

Introduction

IN view of their potential to offer a better control of fuel–air mixture ratio and nitrogen oxides emissions, premixed and partially premixed combustion systems have gained increased attention in recent years. Residential and commercial heating systems operating with natural-gas furnaces are fitted with partially premixed laminar flame burners. These burners are operated with low fuel-supply pressures, typically of the order of a few centimeters of water column, and combustion occurs generally at atmospheric pressure. Hence, the designer's choice of varying operating parameters and flow velocities to control fuel–air mixing rates and pollutant emission characteristics of these burners is severely limited. In this study, a feature of nozzle geometry that can vary fuel–air mixing rates considerably without costly active controls is studied. The fluid mechanics literature contains several documented studies[1–5] that show that air entrainment into isothermal gas jets can be significantly altered by the passive method of using noncircular exit geometries for the nozzle. Thus, the expectation that fuel–air mixing rates, and consequently, combustion and pollutant emission characteristics of reacting fuel gas jets, could be modified by changing the burner exit port geometry from the conventional circular to a noncircular opening, motivated this research. The previous work in the authors' laboratory on noncircular components in gas burners was focused on elliptical geometries. It includes the effects of installing elliptical-shaped components for fuel nozzle,[6] primary air venturi,[7] and burner tip[8] of laminar partially premixed natural gas burners employed in residential and commercial heating systems, and a turbulent diffusion flame.[9] Some improvements in air entrainment, peak temperatures in the flame, and emissions of a few pollutants were noted with the substitution of elliptic components for circular components. A study on the fluid dynamics of jets from sharp-cornered nozzles indicates that the enhancement of small-scale turbulence produced by the corners could provide some additional benefits such as improvement of stability.[3] Being prompted by that result, this study was conducted to understand the flame structure and characteristics of triangular-port burners in partially premixed burners.

Experimental Details

Apparatus

Experiments were conducted in a steel-walled combustion chamber with a square cross section (76 × 76 cm) and 1.22 m height. The chamber was provided with Pyrex® glass windows (20 × 20 × 92 cm) on all four sidewalls. The windows were air-cooled by electrical fans. For introducing thermocouples or gas-sampling probes, one of the windows was replaced by a slotted aluminum plate. The glass windows extended down to the floor level of the chamber to permit optical probing of the flames in the vicinity of the burner exit.

The burner assembly and the gas supply system were designed for a nominal 5.86-kW energy input. The burner assembly consisted of a laminar partially premixed burner producing a vertical flame and interchangeable fuel nozzles, primary air venturis, and exit tips. In this study, the original circular components were retained for fuel nozzle and primary air venturi, and only the burner tip geometry was varied. The standard circular and two modified triangular-shaped tips were investigated. The energy input rate was kept constant in all tests. Figure 1 shows the sketch of the burner and the geometry of the burner tips.

Instrumentation

The apparatus was instrumented for the following measurements: 1) air entrainment, 2) emission indices of pollutants in

Presented as Paper 96-0285 at the AIAA 34th Aerospace Sciences Meeting and Exhibit, Reno, NV, Jan. 15–18, 1996; received Feb. 24, 1996; revision received June 16, 1996; accepted for publication July 11, 1996.

*Lesch Centennial Professor, School of Aerospace and Mechanical Engineering. Associate Fellow AIAA.

†Research Assistant, School of Aerospace and Mechanical Engineering.

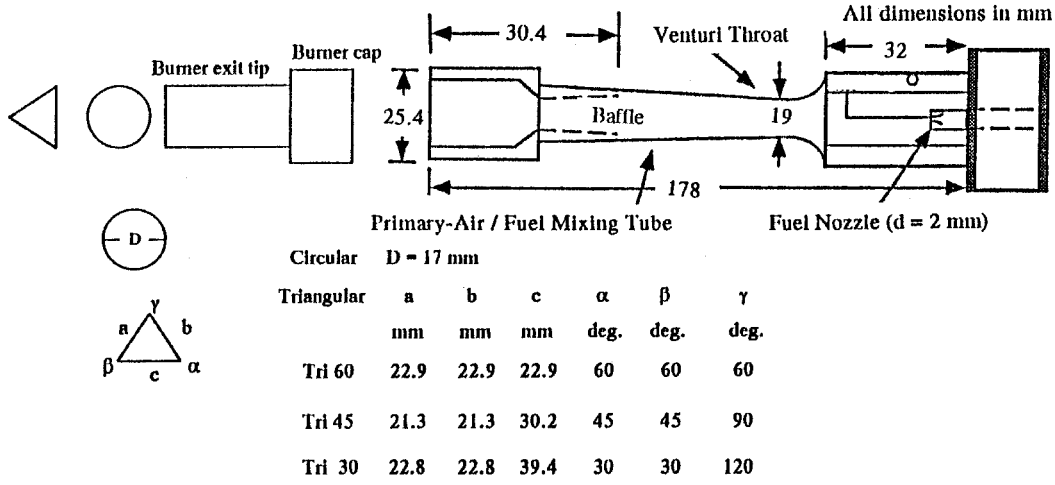

Fig. 1 Sketch of the burner with circular and triangular tips.

exhaust gases, 3) in-flame temperature measurements, 4) in-flame species concentration measurements, and 5) flow visualization. The primary and secondary-air entrainment rates were measured only in nonburning conditions. Oxygen concentration in the jet stream was used as a tracer to obtain the amount of air entrained into the jet. A sequence of quartz probe (1-mm orifice diameter), a vacuum pump, and a polarographic gas analyzer was used to measure oxygen concentration. For primary air entrainment, gas samples were drawn at the burner exit plane to ensure that oxygen present in the jet at that location could be attributed to only the air that was premixed with fuel. For secondary air entrainment, the primary air supply was shut off by enclosing the venturi inlet, and nitrogen was admitted at the same volumetric rate as the primary air. Consequently, the burner exit velocity was kept the same as in the actual operating condition. The gas samples were drawn at several radial locations of the jet cross section at 15 burner exit diameters away from the burner and the average oxygen concentration in that plane was obtained by integrating the radial profiles. The distance of 15 exit diameters was chosen for measuring cumulative air-entrainment in cold jet because it was approximately equal to the flame length. Although the air-entrainment into the flame would be different from that into the cold jet, for the purpose of comparing the burner tip shape effects on air entrainment, measurements were limited to cold jet.

For emission index experiments, a conical Pyrex glass flask open at both ends was mounted directly above the flame. Combustion products of flame were collected and well mixed by this flask as indicated by the uniform temperature and concentration profiles at the exit. Gas samples were withdrawn through a quartz sampling tube and passed through an ice-chilled moisture trap and a series of particulate filters to remove condensed species before the samples were admitted into the analytical instruments. The velocity of the combustion products at the exit of the conical flask was determined using a pitot–static tube and a highly sensitive electronic manometer.

A platinum–platinum/13% rhodium (type R) thermocouple with a butt-welded hot junction of diameter 0.25 mm was used to determine the in-flame and exhaust temperatures. Thermocouple was coated with silica to minimize catalytic effects and the readings were corrected to account for conduction and radiation losses from the hot junction.[10] The in-flame species concentration profiles were also obtained by sampling the gases as described earlier. A chemiluminescent analyzer, a nondispersive infrared detector, and a polarographic analyzer were employed to determine the concentrations of NO/NO_x, CO, and O_2 in the gas samples. The flow visualization of the near-burner region was carried out with shadowgraphic technique, using a mercury light source and 15.2-cm-diam front-surfaced spherical mirror system.

Data Analysis

The primary and secondary air entrainment rates were determined by the mass balance between the exit plane of the fuel nozzle and the plane at which the cumulative air entrainment was desired. As mentioned before, this plane was located at the burner exit for primary air entrainment and at 15D from the burner exit for secondary air entrainment. The molar ratio of the cumulative amount of air entrained into the jet until the plane of the location of measurement n_a to the fuel gas flow rate through the nozzle n_f is given by the equation

$$n_a/n_f = 4.76X_{O_2}/(1 - 4.76X_{O_2}) \quad (1)$$

where X_{O_2} is the mole fraction of oxygen at the plane of measurement.[11]

The emission rates of pollutants from the flames were expressed in terms of an index defined as the mass of the pollutant emitted per unit mass of fuel burned or unit of heat released in the flame. Following Ref. 11, the exhaust concentration of species i emitted per unit mass of fuel burned could be related to the exhaust concentration of CO_2 per unit mass of fuel burned. Since the latter can be accurately calculated if combustion is complete, this method allows the calculation of emission index only by the measurement concentrations of the species i and CO_2 in the products. Thus, the contributions of the errors in measuring the radial profiles of velocities, composition, and temperature of the products in the calculation of the mass rate of species i can be avoided. In this study, the flames were not sooty and the products had very little incomplete combustion products, and hence, the assumption of complete combustion was reasonable. Thus, the emission index of species i, EI_i, was calculated using the following equations[11]:

$$EI_i \text{ (g/kg)} = 1000X_i(M_i)/(16X_{CO_2}) \quad (2)$$

$$EI_i \text{ (ng/J)} = 19{,}764EI_i \text{ (g/kg)}/HHV \quad (3)$$

where M_i is the molecular weight of the species i, and X_i and X_{CO_2} are the mole fractions of the species i and CO_2 in the combustion products, respectively.

Table 1 shows the nominal operating conditions in the experiments of this study. Natural gas (nominal volumetric composition: CH_4 = 92.67%, C_2H_6 = 3.46%, C_3H_8 = 1.10%, CO_2 = 0.45%, C^+ = rest) was used as fuel. Since the composition of natural gas varied slightly over the duration of the study, the heating value of the fuel was determined on a daily basis and the flow rate of fuel was adjusted to maintain the energy input rate to the burner constant. The measurement uncertainties estimated at 95% statistical confidence level using the student's t-test[12] are shown with each figure.

Table 1 Nominal experimental conditions

Fuel, natural gas
HHV, 45.4 MJ/kg
Energy input rate, 5.86 kW
Fuel jet velocity, 49.1 m/s
Fuel jet Re_f, 6500
Burner exit velocity, 1.275 m/s
Burner port Re_p, 3640
Source Fr_p, 6.64
Ambient temperature, 295 K
Ambient pressure, 749 mm Hg
Ambient relative humidity, 65%

Results and Discussion

In the studies presented here, only the burner tip geometry was varied from circular to triangular shapes. Standard circular components were used for the fuel nozzle and primary air venturi. The primary air entrained and premixed with fuel was held constant in this study ($n_{pa}/n_f = 3.5$). Thus, the effects on flame structure and emissions presented can be attributed only to the changes in burner tip geometry.

Air Entrainment

Figure 2 shows the comparison of the rate of secondary air entrainment by the partially premixed fuel–air jet exiting the burner tips of circular and triangular shapes. The graph is presented in a dimensionless form of the entrainment rate for ease of comparison. Because of the difficulties involved in measuring air entrainment rates into the flames, for comparing the effects of burner geometry, the entrainment rates of only nonburning jets were measured. The entrainment rate of a laminar jet is proportional to viscosity of the fluid. Hence, although the absolute values are expected to be smaller in flames, their ratios for different geometries are expected to be similar to the nonburning jet values. The entrainment rate of the circular tip, used as the normalizing value, is also shown with the figure. The jets from triangular burner tips are seen to entrain up to 20% more secondary air. It appears that the equilateral triangle shows the smallest change, and sharper corners produce higher improvement in entrainment rate.

Emission Indices

The emission indices of NO, NO_x, and CO for circular and triangular-shaped nozzles are compared in Fig. 3. The values of emission indices for the circular nozzle are in the range of emission indices noted in the previous studies,[6,7] and are also in agreement with the values expected in practical natural gas heating systems.[13] It is clear that the NO emission decreases markedly when circular tips are replaced by triangular tips. The emission of NO_x also shows a marginal decrease (<10%). However, the CO emission seems to increase by up to 20%. Furthermore, the effect of the sharpness of corners is small.

Temperature Profiles

Figure 4 shows the radial temperature profiles in the flames from circular and triangular ports at three axial distances from the burner exit. These axial locations correspond to the near-burner, midflame, and far-burner regions, where different thermochemical processes dominate the heat-release process. In triangular port flames, the radial profiles were taken along a line passing through the centroid of the triangle. The measurements in Fig. 4 were taken along the direction perpendicular to the major dimension of the triangle. For instance, in the case of Tri 30 port, the measurement direction was perpendicular to the side opposite to the 120-deg included angle. The measurements along the direction perpendicular to the minor dimension of the triangle are given by Subba.[14]

An off-axis double-hump structure exists in the radial temperature profile in the near-nozzle region. The cold fuel in the potential core manifests with a low temperature on the axis. The reaction zone is confined to the edges as the fuel and air diffuse to the interface. That results in the peak temperatures occurring at the edges, leading to the double-hump structure. As the potential core ends, and the fuel pyrolysis/soot formation proceeds, the peaks become flatter in the midflame region. The trends are in agreement with the results of Bar-ziv et al.[15] In the far-nozzle region, where heterogeneous combustion of soot is dominant, only a single axial peak exists. It is seen that, in general, peak temperatures in the near-nozzle and midflame regions are higher than those in the far-nozzle region, which are in agreement with the results of previous studies on circular burner flames. The lower value of peak temperature in the far-nozzle region is caused by the cumulative effect of higher radiant heat losses from that zone, and the dilution caused by air entrainment in excess of that used for combustion. The peak temperatures are in the range of 1400–1600 K, much below the adiabatic flame temperature for methane.[16]

The burner geometry effect on the shapes of temperature profiles appears insignificant, which suggests that the dominant mechanisms of heat release in different regions of the flame are unaltered. Because of the compressed scale in Fig. 4, although the quantitative differences in temperature at all locations are not obvious, the differences in peak values are noticeable. The peak values of temperatures in radial profiles obtained in these tests are shown in Table 2. These data indicate that except for the Tri 30 burner, the changes in the peak temperatures in the near-bumer and midflame regions that occur when the circular tip is replaced by the triangular tips are within the experimental uncertainty. The Tri 30 nozzle with sharp corners substantially lowers the peak temperature in the

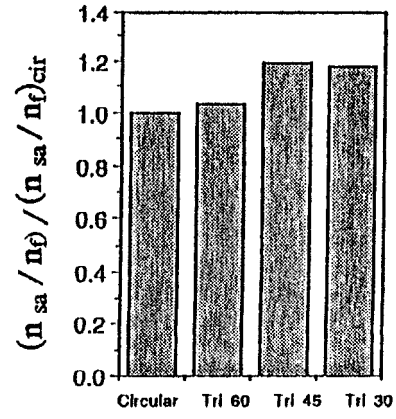

Fig. 2 Relative secondary air entrainment in the nonburning jets: normalizing value for circular port = n_{sa}/n_f = 2.95; estimated maximum uncertainty bandwidth = ±0.012.

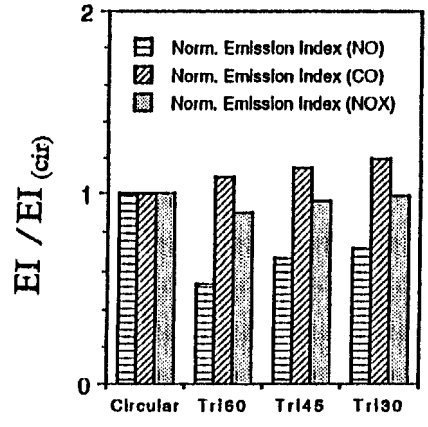

Fig. 3 Relative emission indices from the flames: normalizing values for circular port EI_{NO} = 15 ng/J, EI_{NO_x} = 40 ng/J, and EI_{CO} = 80 ng/J; estimated maximum uncertainty bandwidth = ±0.015.

Table 2 Comparison of peak values in the flames

Measurement	Cir	Tri 60	Tri 45 a	Tri 45 b	Tri 30 a	Tri 30 b
Temperature, K						
Near-nozzle	1540	1600	1545	1535	1440	1470
Midflame	1590	1570	1520	1545	1480	1440
Far-nozzle	1540	1450	1425	1475	1435	1410
NO_x concentration, ppm-v						
Near-nozzle	15	15	17	20	20	28
Midflame	14.5	10	15	19	18	18
Far-nozzle	9.5	7	7.5	9	7.5	8
CO concentration, %-v						
Near-nozzle	1	1.4	1.5	1.75	1.5	1.75
Midflame	1.5	1.2	1.5	1.6	1.5	1.50
Far-nozzle	1	0.8	1.0	0.9	0.8	1.00

a: Along a line passing through the centroid and perpendicular to the major side.
b: Along a line passing through the centroid and perpendicular to the minor side.

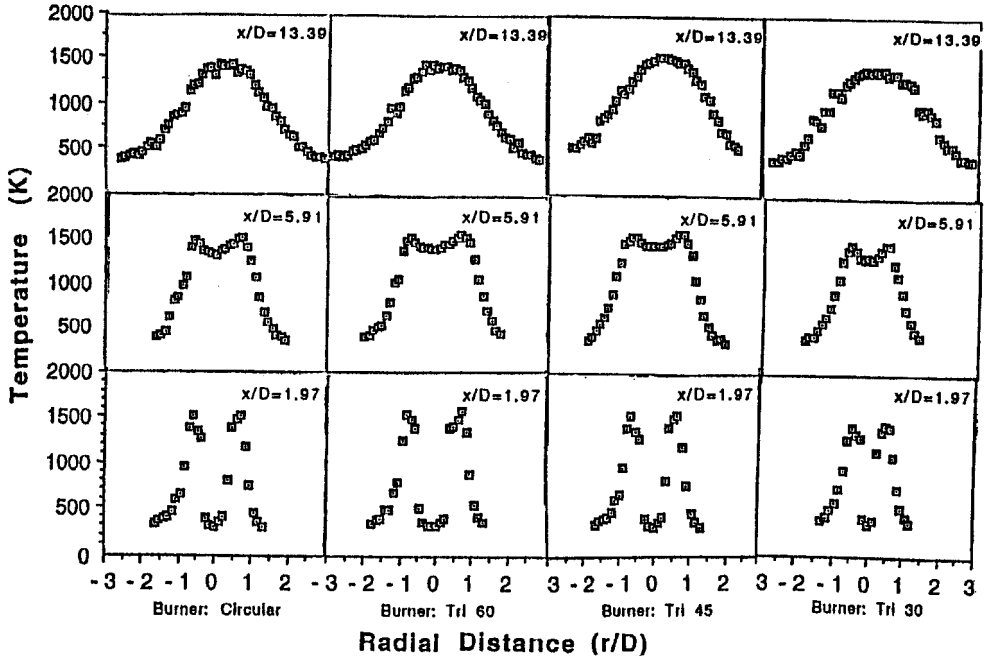

Fig. 4 Radial temperature profiles: for triangular ports in the direction normal to the major side; estimated maximum uncertainty bandwidth = ±30 K.

near-nozzle region. The increase in the small-scale vortices generated at the corners and the locally enhanced mixing and dilution rates may be responsible for the decrease in peak temperature. In the far-nozzle region, however, all triangular tips result in lower peak temperatures compared to the circular tip. The higher cumulative secondary-air entrainment observed in Fig. 2 accounts for this decrease.

Nitrogen Oxide Concentration Profiles

Figure 5 shows the radial concentration profiles of NO_x in different regions of the flames from circular and triangular burner ports. Similar to the data in Figs. 4, these measurements were taken along the directions perpendicular to the major side in the case of triangular ports. A complete set of measurements taken also along the direction perpendicular to the minor dimension, including NO concentrations, is given by Subba.[14]

Similar to the temperature profiles, NO_x concentration profiles also exhibit a double off-axis structure in near-burner and midflame regions. A single axial peak in the far-nozzle region is also seen, although the profiles are flatter in this case. Because the fuel did not contain organically bound nitrogen and most of the nitrogen oxides are formed by the thermal route, the similarity between temperature and NO_x profiles is not surprising. Again, although the quantitative differences are not obvious in these figures, some significant effects of the burner port shape were recorded. The peak values of NO_x concentration in the radial profiles are shown in Table 2. It appears that triangular ports generate more NO_x in the lower regions and smaller amounts in the far-nozzle regions of the flames than the circular ports. Furthermore, in the direction perpendicular to the minor side, the concentrations of NO_x are slightly higher than along the line perpendicular to the major side.

The previous results, in view of the temperature results presented earlier, indicate that the effects of concentrations of species leading to the formation of NO_x are stronger than that of temperature. It appears that the higher degree of turbulence and entrainment rate caused by the sharp corners creates more NO_x in the lower levels of the flame, although the temperature peaks are not affected significantly. This suggests the dominance of reactions of hydrocarbon fragments of fuel pyrolysis, leading to the enhancement of prompt NO in the lower regions of the flame. The relatively weak correlation of temperature and NO_x concentrations in the near-nozzle region supports this argument because of the low sensitivity of nitrogen containing hydrocarbon species reactions to temperature.[17] The higher concentrations of NO_x observed in the direction perpendicular to the minor sides further corroborates this, because the corners generating vorticity that leads to enhanced mixing are closer

to each other in this case than in the direction perpendicular to the major side. In the far-nozzle region, where mostly Zeldovich reactions are the dominant mechanisms, both temperature and NO_x concentrations are lower in the flames with triangular ports.

Carbon Monoxide Concentration Profiles

Figure 6 shows the concentration profiles of carbon monoxide in various regions of flames from circular and triangular burner ports taken along the direction perpendicular to the major side. In the near-burner and midflame regions, the double off-axis peaks exist in the flames of both circular and triangular ports. Since much of the carbon monoxide is formed on the fuel side of the reaction zone in diffusion controlled flames, these profiles are similar to, but narrower than, temperature profiles. A small valley on the flame axis is still noticeable in the far-nozzle profile of the circular port flame, whereas only the axial peak is noticed in the triangular port flames. Because CO is formed by the oxidation of soot in the far-nozzle region, the location of CO concentration peak on the axis indicates that oxygen was penetrating until the axis in the circular port flame. The single axial peak in the triangular port flame is corroborated by the higher air entrainment data presented earlier.

The peak concentrations of CO in radial profiles are shown in Table 2. In the near-burner region, the peak concentration

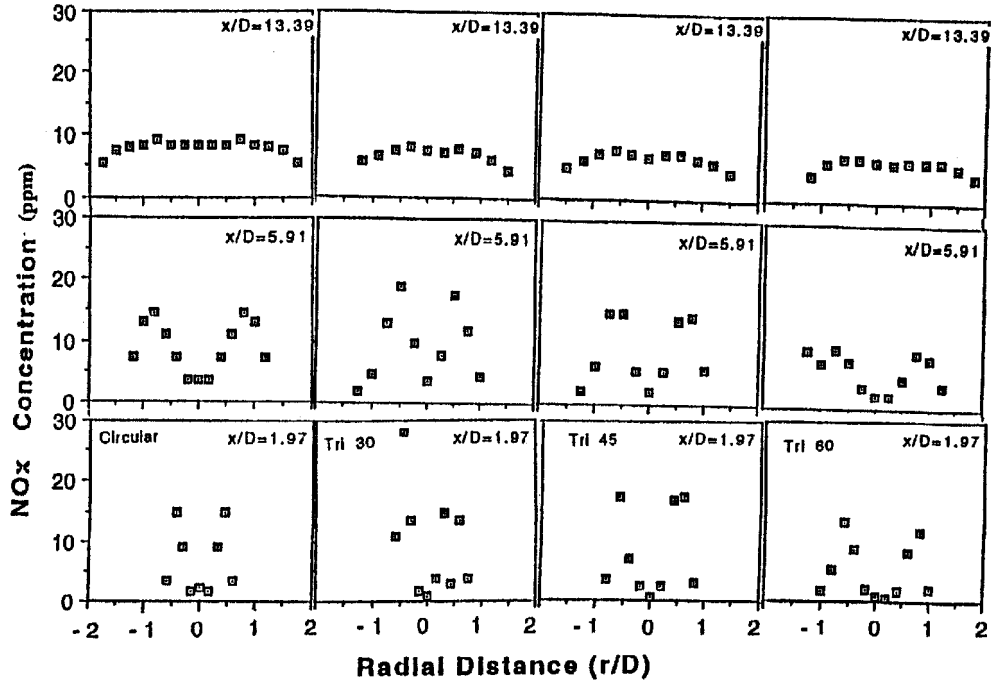

Fig. 5 Radial nitrogen oxides concentration profiles for triangular ports in the direction normal to the major side; estimated maximum uncertainty bandwidth = ±0.5 ppm.

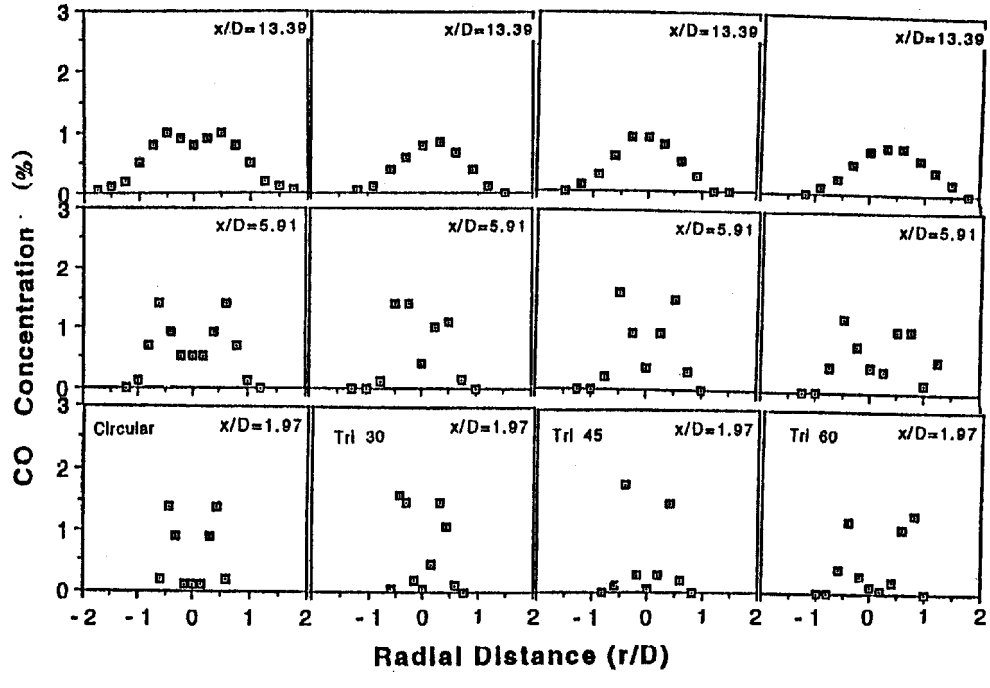

Fig. 6 Radial carbon monoxide concentration profiles for triangular ports in the direction normal to the major side; estimated maximum uncertainty bandwidth = ±0.025%.

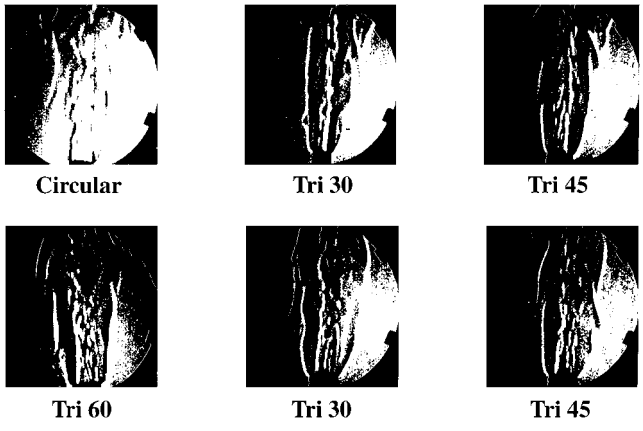

Fig. 7 Shadowgraphs of the near-burner region view for triangular burners: height from the burner exit = 7*D*. Top row, normal to minor side; bottom row, normal to major side.

of CO is higher in the triangular port flames and the effect of port shape on CO concentration in downstream regions appears minimal. The slightly higher CO concentration and approximately the same level of peak temperatures indicate that the entrainment increase is not large enough to convert fuel pyrolysis species completely to CO_2. Hence, the increase in heat release rate is not large enough to compensate the effect of dilution and result in a higher temperature. In the near-burner region, a small increase is seen in the direction perpendicular to the minor side compared to the CO concentration on the direction normal to the major side. Again, the closer proximity of corners and the associated increase in vorticity may be responsible for a slightly higher oxidation rate of the fuel pyrolysis fragments.

Flow Visualization

Figure 7 shows the shadowgraphs of the near-burner region of flames from the circular and triangular ports. For circular and Tri 60 port flames, only one view is shown, and for Tri 45 and Tri 30 port flames, both views perpendicular to the major and minor dimensions are shown. In all flames the jet and the reaction zones are separated by a narrow region, as has previously been observed by different investigators.[18–20] In the circular port flame, because of symmetry, some large-scale coherent structures attributed to Kelvin–Helmholtz-type instability are noticed. Also, the structures appear to begin at approximately 1.5*D* from the port. However, in the triangular port flames, the wavy structure on the inner jet edges does not seem to exist, indicating the coherence is either lost or the size of the structures is reduced. However, the azimuthal instability appears to develop closer to the burner port and is also stronger in the triangular port flames, as indicated by the more numerous streaks in the axial direction. Also, the view perpendicular to the major dimensions of the Tri 45 and Tri 60 ports shows the streaks are denser in the vicinity of the acute angle corners. Thus, the sharp corners of triangular ports result in a higher degree of azimuthal instability, which has been stated to be responsible for higher entrainment rates in elliptic nozzle jets.[5] Furthermore, the scale of the turbulence introduced by these instabilities appears to be finer in triangular port flames, as indicated by the narrower streaks. Thus, the arguments presented in explaining the temperature and concentration results are supported by the flow structure.

Concluding Remarks

This experimental study has shown that flame structure and characteristics are significantly affected by the burner exit port geometry of partially premixed flames of the type employed in small natural-gas-fired heating systems. The differences are more conspicuous in the near-burner region, although the cumulative effects are weakly manifested in the overall flame characteristics. The noncircular shapes introduce more azimuthal instabilities, which result in a higher air entrainment rate. The change in entrainment rate, however, is modest compared to those quoted for highly turbulent jets.[2,5] The reasons can be traced to the fact that the flames in the present study were mostly laminar for over 70% of their length. Some large-scale instabilities leading to flame flickering are noticed in the far field only. The values of Reynolds number and source Froude number based on the area equivalent diameter and exit port conditions were 3.64×10^3 and 6.64, respectively, indicating that the jets were neither momentum controlled nor fully turbulent. Hence, the effects on air entrainment are not as large as in turbulent jets. In flames, the local flow laminarization caused by higher temperatures, as seen in the flame shadowgraphs, is expected to lower the effect of port geometry on air entrainment. Consequently, the basic thermochemical processes are not markedly altered over much of the flame by the port geometry, as seen by the similarity of temperature and concentration profiles in the flames of circular and triangular ports.

Some differences in the peak values of temperature and species concentrations are still evident between the flames of circular and triangular ports. The temperatures in the far-nozzle region are lower in the triangular port flames than in the circular port flames, and the differences are small in the near-burner and midflame regions. The higher air entrainment into the triangular port flames leads to increased gas-phase oxidation reactions and decreased soot formation in the lower flame regions. The combined effect of lower radiation loss from the flame and higher dilution is probably responsible for the small changes in temperatures in the near-burner and midflame regions. Since soot burning is the only dominant heat-releasing process in the far-nozzle regions, a decrease in soot formation in the lower regions decreases heat release in the far-nozzle regions. Also, the higher cumulative air entrainment and dilution result in lower temperatures in the far-nozzle regions of triangular port flames. The higher degree of oxidative reactions caused by the enhanced fuel–air mixing in the near-nozzle region leads to higher peak concentrations of NO_x and CO in that region of triangular port flames. However, the peak concentrations of NO_x in the far-nozzle regions are smaller, whereas the CO concentration does not differ significantly when circular ports are replaced by triangular ports. When the higher mass flow rate of combustion products at the end of the flame are accounted for, these changes in the concentrations result in a small decrease of the emission index of NO_x and a higher emission index of CO. Thus, it appears that in partially premixed laminar burners employed in residential and commercial natural-gas heating systems, triangular-burner ports produce a modest reduction in NO_x emission at the cost of a similar increase in CO emission.

Acknowledgments

This paper was based on the work sponsored by the Gas Research Institute, Contract 5091-260-2178, Chicago, Illinois, under the monitorship of James Kezerle and Robert Serauskas. Also, partial support was provided by the U.S. Department of Energy by Grant DE-FG22-94BC14971.

References

[1]Crighton, D. G., "Instability of an Elliptic Jet," *Journal of Fluid Mechanics*, Vol. 59, Pt. 4, 1973, pp. 665–672.

[2]Gutmark, E., and Ho, C. M., "Visualization of a Forced Elliptic Jet," *AIAA Journal*, Vol. 24, No. 4, 1986, pp. 684, 685.

[3]Gutmark, E., Schadow, K. C., Parr, D. M., Harris, C. K., and Wilson, K. J., "The Mean and Turbulent Structure of Noncircular Jets," AIAA Paper 85-0543, March 1985.

[4]Ho, C. M., and Gutmark, E., "Vortex Induction and Mass Entrainment in a Small Aspect Ratio Elliptic Jet," *Journal of Fluid Mechanics*, Vol. 179, June 1987, pp. 383–405.

[5]Hussain, F., and Hussain, H. S., "Elliptic Jets, Part I Characteristics of Excited and Unexcited Jets," *Journal of Fluid Mechanics*, Vol. 208, Nov. 1989, pp. 257–320.

[6]Kamal, A., and Gollahalli, S. R., "Effects of Noncircular Fuel Nozzles in Inshot Burners of Gas Fired Residential Furnaces," *Combustion Modeling, Cofiring and NO_x Control*, edited by A. K. Gupta et al., Vol. FACT-17, American Society of Mechanical Engineers, New York, 1993, pp. 41–50.

[7]Kolluri, P., Kamal, A., and Gollahalli, S. R., "Application of Elliptical Primary-Air Venturi Inlets Geometries in the Inshot Burners of Residential Gas Furnaces," *Journal of Energy Resources Technology*, Vol. 118, No. 1, 1996, pp. 58–64.

[8]Subba, S., and Gollahalli, S. R., "Flame Structure and Pollutant Emission Characteristics of Noncircular Partially Premixed Laminar Gas Jets," *3rd Asia–Pacific International Symposium on Combustion and Energy Utilization*, Hong Kong Polytechnic Univ., Hung Hom, Kowloon, Hong Kong, 1995, pp. 50–55.

[9]Gollahalli, S. R., Khanna, T., and Prabhu, N., "Diffusion Flames of Gas Jets Issued from Circular and Elliptic Nozzles," *Combustion Science and Technology*, Vol. 86, Nos. 1–6, 1992, pp. 267–290.

[10]Fristrom, R. M., and Westenberg, A. A., *Flame Structure*, McGraw–Hill, New York, 1965.

[11]Gollahalli, S. R., "Research on Combustion Processes Relevant to Burners in HVAC Systems," Gas Research Inst., Final Rept., GRI-94/0420, Chicago, IL, 1994.

[12]Spiegel, M. R., *Theory and Problems of Statistics*, Schaum Publishing Co., New York, 1961.

[13]Levinsky, H. B., "Fundamental Limits of NO and CO Formation in Residential Appliances," Contractors Meeting, Gas Research Inst., Chicago, IL, 1994.

[14]Subba, S., "Effects of Burner Exit Geometry on Combustion Characteristics of Inshot Burners Used in Residential Gas Furnace Systems," M.S. Thesis, Univ. of Oklahoma, Norman, OK, 1995.

[15]Bar-ziv, E., Sgulim, S., Kafri, O., and Keren, E., "Measurement of Temperature Distributions in a Methane-Air Flame by Moire Deflectometry," *19th International Symposium on Combustion*, The Combustion Inst., Pittsburgh, PA, 1982, pp. 303–310.

[16]Kanury, A. M., *Introduction to Combustion Phenomena*, Gordon and Breach, New York, 1975.

[17]Sawyer, R. F., "The Formation and Destruction of Pollutants in Combustion Processes: Clearing the Air on the Role of Combustion Research," *18th International Symposium on Combustion*, The Combustion Inst., Pittsburgh, PA, 1981, pp. 1–22.

[18]Savas, O., and Gollahalli, S. R., "Flow Structure in Near-Nozzle Region of Gas Jet Flames," *AIAA Journal*, Vol. 24, No. 7, 1986, pp. 1137–1140.

[19]Kim, S. J., and Shin, H. D., "A Visual Study of the Structure of Turbulent Nonpremixed Flames near Jet Exit," *Combustion Science and Technology*, Vol. 99, Nos. 1–3, 1994, pp. 37–49.

[20]Clemens, N. T., and Paul, P. H., "Effects of Heat Release on the Near-Field Flow Structure of Hydrogen Gas Jet Diffusion Flames," *Combustion and Flame*, Vol. 102, No. 3, 1995, pp. 271–284.